

Explicit and Implicit Cosimulation Methods: Stability and Convergence Analysis for Different Solver Coupling Approaches

Bernhard Schweizer

Department of Mechanical Engineering,
Institute of Applied Dynamics,
Technical University Darmstadt,
Otto-Berndt-Strasse 2,
Darmstadt 64287, Germany
e-mail: schweizer@sds.tu-darmstadt.de

Pu Li

Department of Mechanical Engineering,
Institute of Applied Dynamics,
Technical University Darmstadt,
Otto-Berndt-Strasse 2,
Darmstadt 64287, Germany

Daixing Lu

Department of Mechanical Engineering,
Institute of Applied Dynamics,
Technical University Darmstadt,
Otto-Berndt-Strasse 2,
Darmstadt 64287, Germany

The numerical stability and the convergence behavior of cosimulation methods are analyzed in this manuscript. We investigate explicit and implicit coupling schemes with different approximation orders and discuss three decomposition techniques, namely, force/force-, force/displacement-, and displacement/displacement-decomposition. Here, we only consider cosimulation methods where the coupling is realized by applied forces/torques, i.e., the case that the coupling between the subsystems is described by constitutive laws. Solver coupling with algebraic constraint equations is not investigated. For the stability analysis, a test model has to be defined. Following the stability definition for numerical time integration schemes (Dahlquist's stability theory), a linear test model is used. The cosimulation test model applied here is a two-mass oscillator, which may be interpreted as two Dahlquist equations coupled by a linear spring/damper system. Discretizing the test model with a cosimulation method, recurrence equations can be derived, which describe the time discrete cosimulation solution. The stability of the recurrence equations system represents the numerical stability of the cosimulation approach and can easily be determined by an eigenvalue analysis. [DOI: 10.1115/1.4028503]

Keywords: cosimulation, solver coupling, parallelization, subcycling, explicit, implicit, coupling by constitutive laws, stability, convergence

1 Introduction

Cosimulation or solver coupling is used to couple two or more solvers in time domain. Different numerical techniques have been developed and applied in various fields of applications. Solver coupling has successfully been used in the field of vehicle dynamics [1–4], in connection with fluid/structure interaction problems [5–8] or for the combined simulation of multibody and finite-element systems [9–11]. The coupled simulation of multibody and hydraulic systems in the framework of a cosimulation approach is, for instance, discussed in Refs. [12] and [13]. Interaction problems including particle and multibody models are investigated in Refs. [14–16].

The basic idea behind a cosimulation approach consists in a decomposition of the overall system into two (or more) subsystems. Basically, two methods exist to define the coupling between the subsystems. On the one hand, the coupling of the subsystems may be described by physical force/torque laws (constitutive laws) so that applied forces/torques are used to connect the subsystems [17–21]. On the other hand, the subsystem coupling can be specified by algebraic constraint equations so that reaction forces/torques are used to connect the subsystems [22–26]. With respect to the decomposition of the overall system into subsystems, three different techniques can be distinguished: The force/force-, the force/displacement-, and the displacement/displacement-decomposition approach [17,27,28]. In this manuscript, cosimulation approaches based on an equidistant communication time grid are examined, i.e., the macrostep size is assumed to be constant. Coupling approaches with variable macrostep sizes are, for instance, discussed in Refs. [29,30].

Contributed by the Design Engineering Division of ASME for publication in the JOURNAL OF COMPUTATIONAL AND NONLINEAR DYNAMICS. Manuscript received March 5, 2014; final manuscript received September 3, 2014; published online April 2, 2015. Assoc. Editor: Dan Negru.

In order to define and investigate the numerical stability of cosimulation methods, it is useful to adopt and extend the theory developed for time integration schemes [31,32]. The stability of numerical time integration methods is defined by Dahlquist's test equation

$$\dot{y}(t) = \lambda \cdot y(t) \quad (1)$$

where $y(t)$ is a scalar function of time and $\lambda \in \mathbb{C}$ an arbitrary complex constant. Note that $\dot{y} = (dy/dt)$ terms the derivative of y with respect to time t . Dahlquist's test equation may—from the mechanical point of view—be interpreted as the complex representation of the equations of motion for the linear single-mass oscillator. This can be easily seen by considering the linear homogenous mass–spring–damper oscillator, which is mathematically described by

$$\begin{pmatrix} \dot{x} \\ \dot{v} \end{pmatrix} = \begin{pmatrix} 0 & 1 \\ -\frac{c}{m} & -\frac{d}{m} \end{pmatrix} \begin{pmatrix} x \\ v \end{pmatrix} \quad (2)$$

where x and v denote the position and the velocity of the mass m . c and d term the spring constant and the damping coefficient. With the (complex) eigenvalues $\lambda_{1,2} = \lambda_r \pm i \cdot \lambda_i = -(d/(2 \cdot m)) \pm i \cdot (\sqrt{4 \cdot m \cdot c - d^2}/(2 \cdot m))$ of the system matrix, with the modal matrix $\mathcal{Q} = \begin{pmatrix} 1 & 1 \\ \lambda_1 & \lambda_2 \end{pmatrix}$ containing the eigenvectors and with the new coordinates $\begin{pmatrix} y_1 \\ y_2 \end{pmatrix} = \mathcal{Q}^{-1} \begin{pmatrix} x \\ v \end{pmatrix}$, system (2) can be transformed into the two decoupled equations

$$\begin{pmatrix} \dot{y}_1 \\ \dot{y}_2 \end{pmatrix} = \begin{pmatrix} \lambda_1 & 0 \\ 0 & \lambda_2 \end{pmatrix} \begin{pmatrix} y_1 \\ y_2 \end{pmatrix} \quad (3)$$

Discretizing the Dahlquist equation (1) with a linear single-step (e.g., Runge–Kutta method) or a linear multistep method (e.g., Adams–Bashforth method) and assuming a constant step size h yields a recurrence equation for the discretized values y_n ($n = 0, 1, 2, \dots$), which approximate the analytical solution $y(t_n)$ at the time points t_n . Provided that $m, c, d > 0$ (i.e., assuming that the system is stable from the mechanical point of view), a numerical time integration method is called numerically stable, if the discretized Dahlquist equation (1) yields a sequence of exponentially decaying values y_n . This will be the case if the spectral radius of the recurrence equation is smaller than 1. As well known from literature, the stability behavior of a time integration method depends on two parameters, namely, $h\lambda_r$ and $h\lambda_i$. Since the spectral radius is only a function of two parameters, results of stability analyses can easily be illustrated in 2D stability plots.

To examine the stability of cosimulation methods, it is quite obvious to use the linear two-mass oscillator as test model, see Fig. 1. The two-mass oscillator can be interpreted as two single-mass oscillators (masses m_1/m_2 , spring constants c_1/c_2 , and damping coefficients d_1/d_2), which are coupled by the coupling spring c_c and the coupling damper d_c . Hence, the two-mass oscillator can be regarded as two Dahlquist equations, which are coupled by a linear spring/damper system.

The equations of motion for the coupled oscillator read as

$$\begin{aligned}\dot{x}_1 &= v_1 \\ \dot{v}_1 &= -\frac{c_1}{m_1}x_1 - \frac{d_1}{m_1}v_1 + \frac{c_c}{m_1} \cdot (x_2 - x_1) + \frac{d_c}{m_1} \cdot (v_2 - v_1) \\ \dot{x}_2 &= v_2 \\ \dot{v}_2 &= -\frac{c_2}{m_2}x_2 - \frac{d_2}{m_2}v_2 - \frac{c_c}{m_2} \cdot (x_2 - x_1) - \frac{d_c}{m_2} \cdot (v_2 - v_1)\end{aligned}\quad (4)$$

where x_1/x_2 and v_1/v_2 describe position and velocity of the two masses.

For the stability analysis of cosimulation methods, it is useful to introduce the dimensionless time $\bar{t} = (t/H)$, where H denotes the macrostep size of the cosimulation approach, see Sec. 2. Moreover, it is suitable to define the following seven parameters:

$$\begin{aligned}\bar{c}_1 &= \frac{c_1 \cdot H^2}{m_1}, \quad \bar{d}_1 = \frac{d_1 \cdot H}{m_1}, \quad \alpha_{m21} = \frac{m_2}{m_1}, \\ \alpha_{c21} &= \frac{c_2}{c_1}, \quad \alpha_{d21} = \frac{d_2}{d_1}, \quad \alpha_{cc1} = \frac{c_c}{c_1}, \quad \alpha_{dc1} = \frac{d_c}{d_1}\end{aligned}\quad (5)$$

With these parameters, Eq. (4) can be rewritten as

$$\begin{aligned}x'_1 &= \bar{v}_1 \\ \bar{v}'_1 &= -\bar{c}_1 \cdot x_1 - \bar{d}_1 \cdot \bar{v}_1 + \alpha_{cc1} \cdot \bar{c}_1 \cdot (x_2 - x_1) + \alpha_{dc1} \cdot \bar{d}_1 \cdot (\bar{v}_2 - \bar{v}_1) \\ x'_2 &= \bar{v}_2 \\ \bar{v}'_2 &= -\frac{\alpha_{c21}}{\alpha_{m21}} \cdot \bar{c}_1 \cdot x_2 - \frac{\alpha_{d21}}{\alpha_{m21}} \cdot \bar{d}_1 \cdot \bar{v}_2 - \frac{\alpha_{cc1}}{\alpha_{m21}} \cdot \bar{c}_1 \cdot (x_2 - x_1) \\ &\quad - \frac{\alpha_{dc1}}{\alpha_{m21}} \cdot \bar{d}_1 \cdot (\bar{v}_2 - \bar{v}_1)\end{aligned}\quad (6)$$

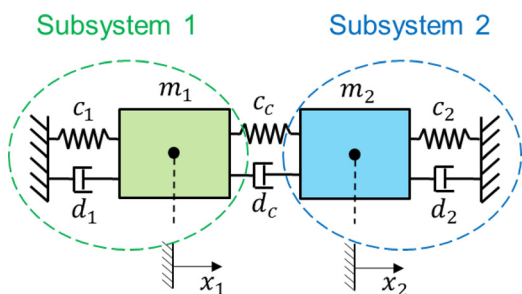


Fig. 1 Linear two-mass oscillator: test model for analyzing the stability of cosimulation methods

In the above equation, $(\cdot)' = (d(\cdot)/d\bar{t})$ terms the derivative with respect to the dimensionless time \bar{t} . $\bar{v}_1 = H \cdot v_1$ and $\bar{v}_2 = H \cdot v_2$ denote modified (dimensionless) velocities. Note that for $m_1, m_2, c_1, c_2, c_c, d_1, d_2, d_c > 0$, the two-mass oscillator is a stable system from the mechanical point of view. Discretization of Eq. (6) with a linear cosimulation method yields a linear homogeneous system of recurrence equations, see Sec. 2. The stability of this recurrence equations system—and as a consequence the stability of the underlying cosimulation method—can easily be determined by calculating the spectral radius of the recurrence equations system. If the spectral radius is smaller than 1, the cosimulation is called numerically stable. The spectral radius depends on seven independent parameters, see Eq. (5). For a graphical representation, it is useful to fix five parameters so that the spectral radius can be plotted in 2D diagrams as a function of the remaining two parameters.

As mentioned above, we only discuss solver coupling methods based on constitutive laws in this manuscript. It should be pointed out that for constraint coupling approaches, the above presented seven-parameter cosimulation test model is not appropriate. As outlined in Ref. [26], a one degree of freedom cosimulation test model with five parameters, which represents two algebraically coupled Dahlquist equations, has to be used for the stability analysis of cosimulation methods with algebraic constraints.

This paper is organized as follows: Based on the cosimulation test model, the recurrence equations systems, which describe the numerical stability of the explicit and implicit cosimulation approaches considered here, are derived in Sec. 2. Stability and convergence plots are presented in Sec. 3. Results are summarized in Sec. 4.

2 Test Model and Recurrence Equations Systems for Implicit and Explicit Cosimulation Methods

Applying a cosimulation approach, the overall system is split into two (or more) subsystems by using a force/force-, a force/displacement- or a displacement/displacement-decomposition technique [17,27,28]. To simulate the decoupled system in the framework of a cosimulation approach, coupling variables (subsystem input and output variables) have to be specified and a macrotime grid (macrotime points T_0, T_1, \dots, T_N) has to be defined. In this work, an equidistant macrotime grid is used so that the macrostep size $H = T_{N+1} - T_N$ is constant. Making use of a cosimulation method (weak coupling approach) [18,33], the two subsystems integrate independently between the macrotime points. The coupling variables are only exchanged between the subsystems at the macrotime points. For integrating the subsystems from one to the next macrotime point ($T_N \rightarrow T_{N+1}$), the coupling variables have to be approximated using extrapolation/interpolation techniques. In this paper, Lagrange polynomials are used for approximating the coupling variables.

In Secs. 2.1–2.3, we investigate implicit and explicit coupling approaches for the three decomposition techniques. Here, we assume that the subsystems are integrated in parallel (Jacobi type). Serial integration schemes (Gauss–Seidel type) are not discussed, but may be treated in a very similar manner.

2.1 Force/Force-Coupling

2.1.1 Implicit Cosimulation Approach. By applying a force/force-decomposition technique, the cosimulation test model is split into two subsystems in such a way that both subsystems are force-driven single-mass oscillators, see Fig. 2. The two masses are driven by the coupling force λ_c . The coupling force is a function of the state variables of the subsystems and can be defined by the implicit coupling condition $g_{c\lambda} := \lambda_c - \lambda_c \cdot (x_2 - x_1) - d_c \cdot (v_2 - v_1) = 0$.

Using the modified (dimensionless) velocity variables and the parameters from Eq. (5), the decomposed system is described by the following semi-explicit index-1 DAE (differential algebraic equation) system:

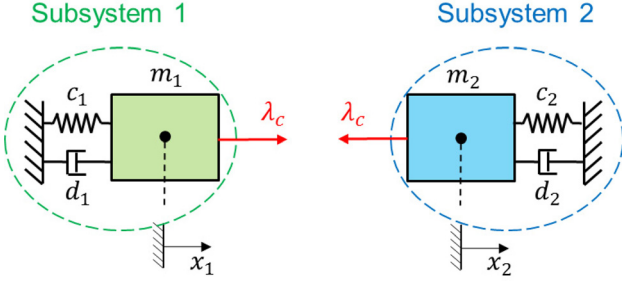


Fig. 2 Cosimulation test model: force/force-coupling approach

Subsystem 1:

$$\begin{aligned} x'_1 &= \bar{v}_1 \\ \bar{v}'_1 &= -\bar{c}_1 \cdot x_1 - \bar{d}_1 \cdot \bar{v}_1 + \bar{\lambda}_c \end{aligned} \quad (7a)$$

Subsystem 2:

$$\begin{aligned} x'_2 &= \bar{v}_2 \\ \bar{v}'_2 &= -\frac{\alpha_{c21}}{\alpha_{m21}} \cdot \bar{c}_1 \cdot x_2 - \frac{\alpha_{d21}}{\alpha_{m21}} \cdot \bar{d}_1 \cdot \bar{v}_2 - \frac{1}{\alpha_{m21}} \bar{\lambda}_c \end{aligned} \quad (7b)$$

Coupling condition:

$$\bar{g}_{c\lambda} := \bar{\lambda}_c - \alpha_{cc1} \cdot \bar{c}_1 \cdot (x_2 - x_1) - \alpha_{dc1} \cdot \bar{d}_1 \cdot (\bar{v}_2 - \bar{v}_1) = 0 \quad (7c)$$

It should be mentioned that $\bar{\lambda}_c = (\lambda_c \cdot H^2/m_1)$ represents the modified (dimensionless) coupling force. To derive the recurrence equations system for the discretized test model, we consider the general macrostep from \bar{T}_N to \bar{T}_{N+1} . Note that $\bar{T}_N = (T_N/H)$ terms the dimensionless macrotime point. For integrating the subsystems from \bar{T}_N to \bar{T}_{N+1} , the coupling variable $\bar{\lambda}_c(\bar{t})$ has to be approximated in the time interval $[\bar{T}_N, \bar{T}_{N+1}]$. Therefore, Lagrange polynomials of degree k are used, which are specified by $k+1$ sampling points. Using, for instance, the $k+1$ sampling points $(\bar{T}_N, \bar{\lambda}_{c,N}), (\bar{T}_{N-1}, \bar{\lambda}_{c,N-1}), \dots, (\bar{T}_{N-k}, \bar{\lambda}_{c,N-k})$, we get a polynomial of degree k , which we abbreviate by $P_{\bar{\lambda}_c}[(\bar{T}_N, \bar{\lambda}_{c,N}), (\bar{T}_{N-1}, \bar{\lambda}_{c,N-1}), \dots, (\bar{T}_{N-k}, \bar{\lambda}_{c,N-k}); \bar{t}]$.

At the beginning of the macrotime step, the state variables and the coupling variable are assumed to be known

$$x_1(\bar{t} = \bar{T}_N) = x_{1,N}, \quad \bar{v}_1(\bar{t} = \bar{T}_N) = \bar{v}_{1,N} \quad (8a)$$

$$x_2(\bar{t} = \bar{T}_N) = x_{2,N}, \quad \bar{v}_2(\bar{t} = \bar{T}_N) = \bar{v}_{2,N} \quad (8b)$$

$$\bar{\lambda}_c(\bar{t} = \bar{T}_N) = \bar{\lambda}_{c,N} \quad (8b)$$

For higher order approximation ($k > 0$), we further assume that the coupling variable is known at the previous k macrotime points $\bar{T}_{N-1}, \dots, \bar{T}_{N-k}$.

The implicit cosimulation approaches considered here are predictor/corrector approaches, which can be subdivided into three steps. Below, predicted variables are indicated with an upper index p (e.g., $x_{1,N+1}^p$). Variables without upper index are assumed to be corrected variables (e.g., $x_{1,N+1}$). For the following analysis, it is useful to define the vectors $\mathbf{z}_N = (x_{1,N}, \bar{v}_{1,N}, x_{2,N}, \bar{v}_{2,N})^\top$, $\mathbf{z}_{N-1} = (x_{1,N-1}, \bar{v}_{1,N-1}, x_{2,N-1}, \bar{v}_{2,N-1})^\top, \dots, \mathbf{z}_{N-k} = (x_{1,N-k}, \bar{v}_{1,N-k}, x_{2,N-k}, \bar{v}_{2,N-k})^\top$, which collect the state variables of both subsystems at the macrotime points $\bar{T}_N, \bar{T}_{N-1}, \dots, \bar{T}_{N-k}$.

Step 1: Predictor Step

- An analytical integration of subsystem 1 and subsystem 2 from \bar{T}_N to \bar{T}_{N+1} with initial conditions (8a) and with the predictor (extrapolation) polynomial

$$\bar{\lambda}_c^p(\bar{t}) = P_{\bar{\lambda}_c}^p[(\bar{T}_N, \bar{\lambda}_{c,N}), (\bar{T}_{N-1}, \bar{\lambda}_{c,N-1}), \dots, (\bar{T}_{N-k}, \bar{\lambda}_{c,N-k}); \bar{t}] \quad (9)$$

yields predicted state variables at the macrotime point \bar{T}_{N+1}

$$\begin{aligned} x_{1,N+1}^p &= x_{1,N+1}^p(\bar{\lambda}_{c,N}, \bar{\lambda}_{c,N-1}, \dots, \bar{\lambda}_{c,N-k}, \mathbf{z}_N) \\ \bar{v}_{1,N+1}^p &= \bar{v}_{1,N+1}^p(\bar{\lambda}_{c,N}, \bar{\lambda}_{c,N-1}, \dots, \bar{\lambda}_{c,N-k}, \mathbf{z}_N) \\ x_{2,N+1}^p &= x_{2,N+1}^p(\bar{\lambda}_{c,N}, \bar{\lambda}_{c,N-1}, \dots, \bar{\lambda}_{c,N-k}, \mathbf{z}_N) \\ \bar{v}_{2,N+1}^p &= \bar{v}_{2,N+1}^p(\bar{\lambda}_{c,N}, \bar{\lambda}_{c,N-1}, \dots, \bar{\lambda}_{c,N-k}, \mathbf{z}_N) \end{aligned} \quad (10)$$

Step 2: Calculation of Corrected Coupling Force

- By analytically integrating subsystem 1 and subsystem 2 from \bar{T}_N to \bar{T}_{N+1} with initial conditions (8a) and using the interpolation polynomial

$$\bar{\lambda}_c^*(\bar{t}) = P_{\bar{\lambda}_c}^*[(\bar{T}_{N+1}, \bar{\lambda}_{c,N+1}^*), (\bar{T}_N, \bar{\lambda}_{c,N}), \dots, (\bar{T}_{N-k+1}, \bar{\lambda}_{c,N-k+1}); \bar{t}] \quad (11)$$

we get the following state variables at the macrotime point \bar{T}_{N+1} :

$$\begin{aligned} x_{1,N+1}^* &= x_{1,N+1}^*(\bar{\lambda}_{c,N+1}^*, \bar{\lambda}_{c,N}, \dots, \bar{\lambda}_{c,N-k+1}, \mathbf{z}_N) \\ \bar{v}_{1,N+1}^* &= \bar{v}_{1,N+1}^*(\bar{\lambda}_{c,N+1}^*, \bar{\lambda}_{c,N}, \dots, \bar{\lambda}_{c,N-k+1}, \mathbf{z}_N) \\ x_{2,N+1}^* &= x_{2,N+1}^*(\bar{\lambda}_{c,N+1}^*, \bar{\lambda}_{c,N}, \dots, \bar{\lambda}_{c,N-k+1}, \mathbf{z}_N) \\ \bar{v}_{2,N+1}^* &= \bar{v}_{2,N+1}^*(\bar{\lambda}_{c,N+1}^*, \bar{\lambda}_{c,N}, \dots, \bar{\lambda}_{c,N-k+1}, \mathbf{z}_N) \end{aligned} \quad (12)$$

Please note that $\bar{\lambda}_{c,N+1}^*$ represents an arbitrary coupling force at the macrotime point \bar{T}_{N+1} .

- Differentiating the state variables of Eq. (12) with respect to $\bar{\lambda}_{c,N+1}^*$, we obtain the partial derivatives

$$\begin{aligned} \frac{\partial x_{1,N+1}^*}{\partial \bar{\lambda}_{c,N+1}^*} &= \text{const.}, \quad \frac{\partial \bar{v}_{1,N+1}^*}{\partial \bar{\lambda}_{c,N+1}^*} = \text{const.} \\ \frac{\partial x_{2,N+1}^*}{\partial \bar{\lambda}_{c,N+1}^*} &= \text{const.}, \quad \frac{\partial \bar{v}_{2,N+1}^*}{\partial \bar{\lambda}_{c,N+1}^*} = \text{const.} \end{aligned} \quad (13)$$

Note that the partial derivatives are constant, because the state variables of Eq. (12) only depend linearly on $\bar{\lambda}_{c,N+1}^*$.

- Making use of the partial derivatives, a corrected coupling force $\bar{g}_{c\lambda,N+1}$, which fulfills the coupling condition (7c) at the macrotime point \bar{T}_{N+1} can be computed. Regarding the fixed time point \bar{T}_{N+1} , $\bar{g}_{c\lambda,N+1}$ may be considered as a function of the coupling force $\bar{\lambda}_{c,N+1}^*$

$$\begin{aligned} \bar{g}_{c\lambda,N+1}(\bar{\lambda}_{c,N+1}^*) &:= \bar{\lambda}_{c,N+1}^* - \alpha_{cc1} \cdot \bar{c}_1 \cdot (x_{2,N+1}^*(\bar{\lambda}_{c,N+1}^*) \\ &\quad - x_{1,N+1}^*(\bar{\lambda}_{c,N+1}^*)) - \alpha_{dc1} \cdot \bar{d}_1 \cdot (\bar{v}_{2,N+1}^*(\bar{\lambda}_{c,N+1}^*) \\ &\quad - \bar{v}_{1,N+1}^*(\bar{\lambda}_{c,N+1}^*)) \end{aligned} \quad (14)$$

Since the state variables $x_{1,N+1}^*, x_{2,N+1}^*, \bar{v}_{1,N+1}^*$, and $\bar{v}_{2,N+1}^*$ depend only linearly on $\bar{\lambda}_{c,N+1}^*$, Eq. (14) can be rewritten as

$$\begin{aligned} \bar{g}_{c\lambda,N+1}(\bar{\lambda}_{c,N+1}^p) &:= \bar{g}_{c\lambda,N+1}(\bar{\lambda}_{c,N+1}^p) \\ &\quad + \left. \frac{\partial \bar{g}_{c\lambda,N+1}}{\partial \bar{\lambda}_{c,N+1}^*} \right|_{\bar{\lambda}_{c,N+1}^p} \cdot (\bar{\lambda}_{c,N+1}^* - \bar{\lambda}_{c,N+1}^p) \\ &= \bar{\lambda}_{c,N+1}^p - \alpha_{cc1} \cdot \bar{c}_1 \cdot (x_{2,N+1}^*(\bar{\lambda}_{c,N+1}^p) - x_{1,N+1}^*(\bar{\lambda}_{c,N+1}^p)) \\ &\quad - \alpha_{dc1} \cdot \bar{d}_1 \cdot (\bar{v}_{2,N+1}^*(\bar{\lambda}_{c,N+1}^p) - \bar{v}_{1,N+1}^*(\bar{\lambda}_{c,N+1}^p)) \\ &\quad + \left[1 - \alpha_{cc1} \cdot \bar{c}_1 \cdot \left(\frac{\partial x_{2,N+1}^*}{\partial \bar{\lambda}_{c,N+1}^*} - \frac{\partial x_{1,N+1}^*}{\partial \bar{\lambda}_{c,N+1}^*} \right) \right. \\ &\quad \left. - \alpha_{dc1} \cdot \bar{d}_1 \cdot \left(\frac{\partial \bar{v}_{2,N+1}^*}{\partial \bar{\lambda}_{c,N+1}^*} - \frac{\partial \bar{v}_{1,N+1}^*}{\partial \bar{\lambda}_{c,N+1}^*} \right) \right] \cdot (\bar{\lambda}_{c,N+1}^* - \bar{\lambda}_{c,N+1}^p) \end{aligned} \quad (15)$$

where $\bar{\lambda}_{c,N+1}^p = \bar{\lambda}_c^p(\bar{T}_{N+1})$ terms the predicted coupling force at \bar{T}_{N+1} .

- By setting $\bar{g}_{c\lambda,N+1}\left(\bar{\lambda}_{c,N+1}^*\right) = 0$, we get the corrected coupling force

$$\bar{\lambda}_{c,N+1} = \bar{\lambda}_{c,N+1}^p - \frac{\bar{\lambda}_{c,N+1}^p - \alpha_{cc1} \cdot \bar{c}_1 \cdot \left(x_{2,N+1}(\bar{\lambda}_{c,N+1}^p) - x_{1,N+1}(\bar{\lambda}_{c,N+1}^p) \right) - \alpha_{dc1} \cdot \bar{d}_1 \cdot \left(\bar{v}_{2,N+1}(\bar{\lambda}_{c,N+1}^p) - \bar{v}_{1,N+1}(\bar{\lambda}_{c,N+1}^p) \right)}{\left[1 - \alpha_{cc1} \cdot \bar{c}_1 \cdot \left(\frac{\partial \lambda_{2,N+1}^*}{\partial \bar{\lambda}_{c,N+1}^*} - \frac{\partial x_{1,N+1}^*}{\partial \bar{\lambda}_{c,N+1}^*} \right) - \alpha_{dc1} \cdot \bar{d}_1 \cdot \left(\frac{\partial \bar{v}_{2,N+1}^*}{\partial \bar{\lambda}_{c,N+1}^*} - \frac{\partial \bar{v}_{1,N+1}^*}{\partial \bar{\lambda}_{c,N+1}^*} \right) \right]} \quad (16)$$

Please note that for the reason of a clear representation, different variables have been used for the general coupling force $\bar{\lambda}_{c,N+1}^*$ at the time point \bar{T}_{N+1} and the corrected coupling force $\bar{\lambda}_{c,N+1}$, which represents the root of Eq. (15).

Step 3: Corrector Step

- Using an interpolation polynomial with the corrected coupling force $\bar{\lambda}_{c,N+1}$ from Eq. (16), an analytical integration of subsystem 1 and subsystem 2 from \bar{T}_N to \bar{T}_{N+1} with initial conditions (8a) gives the corrected states

$$\begin{aligned} x_{1,N+1} &= x_{1,N+1}(\bar{\lambda}_{c,N+1}, \bar{\lambda}_{c,N}, \dots, \bar{\lambda}_{c,N-k+1}, z_N) \\ \bar{v}_{1,N+1} &= \bar{v}_{1,N+1}(\bar{\lambda}_{c,N+1}, \bar{\lambda}_{c,N}, \dots, \bar{\lambda}_{c,N-k+1}, z_N) \\ x_{2,N+1} &= x_{2,N+1}(\bar{\lambda}_{c,N+1}, \bar{\lambda}_{c,N}, \dots, \bar{\lambda}_{c,N-k+1}, z_N) \\ \bar{v}_{2,N+1} &= \bar{v}_{2,N+1}(\bar{\lambda}_{c,N+1}, \bar{\lambda}_{c,N}, \dots, \bar{\lambda}_{c,N-k+1}, z_N) \end{aligned} \quad (17)$$

With the help of the corrected state variables from Eq. (17), it is straightforward to derive recurrence equations, which only contain the state variables at the current and previous macrotime points. Evaluating the coupling condition at the $k+1$ macrotime points $\bar{T}_{N+1}, \dots, \bar{T}_{N-k+1}$ yields

$$\begin{aligned} \bar{\lambda}_{c,N+1} &= \alpha_{cc1} \cdot \bar{c}_1 \cdot (x_{2,N+1} - x_{1,N+1}) \\ &\quad + \alpha_{dc1} \cdot \bar{d}_1 \cdot (\bar{v}_{2,N+1} - \bar{v}_{1,N+1}) \\ &\quad \vdots \\ \bar{\lambda}_{c,N-k+1} &= \alpha_{cc1} \cdot \bar{c}_1 \cdot (x_{2,N-k+1} - x_{1,N-k+1}) \\ &\quad + \alpha_{dc1} \cdot \bar{d}_1 \cdot (\bar{v}_{2,N-k+1} - \bar{v}_{1,N-k+1}) \end{aligned} \quad (18)$$

Making use of Eq. (18), the coupling forces $\bar{\lambda}_{c,N+1}, \dots, \bar{\lambda}_{c,N-k+1}$ can be eliminated in Eq. (17), which results in relationships of the form

$$\begin{aligned} x_{1,N+1} &= x_{1,N+1}(z_{N+1}, z_N, \dots, z_{N-k+1}) \\ \bar{v}_{1,N+1} &= \bar{v}_{1,N+1}(z_{N+1}, z_N, \dots, z_{N-k+1}) \\ x_{2,N+1} &= x_{2,N+1}(z_{N+1}, z_N, \dots, z_{N-k+1}) \\ \bar{v}_{2,N+1} &= \bar{v}_{2,N+1}(z_{N+1}, z_N, \dots, z_{N-k+1}) \end{aligned} \quad (19)$$

Equation (19) represents a system of four coupled linear recurrence equations. This system can symbolically be written as

$$A_{N+1} \cdot z_{N+1} + A_N \cdot z_N + \dots + A_{N-k+1} \cdot z_{N-k+1} = 0 \quad (20)$$

The real-valued matrices $A_{N+1}, \dots, A_{N-k+1} \in \mathbb{R}^{4 \times 4}$ are constant and only depend on the seven parameters of the cosimulation test model.

Since the subsystem integration is carried out analytically, the stability behavior of the cosimulation approach is directly determined by the stability of the linear recurrence equations system

(20). This system can easily be solved by the exponential approach $z_N = \hat{z} \cdot \hat{\lambda}^N$, where $\hat{\lambda}$ denotes the eigenvalue and \hat{z} the eigenvector of the system. The recurrence system (20) has in general $j = 1, \dots, 4 \cdot k$ eigenvalues and corresponding eigenvectors. If the spectral radius $\rho = \max\{|\lambda_j|\}$ —i.e., the magnitude of the largest eigenvalue—is larger than 1, the cosimulation becomes unstable. Since the matrices $A_{N+1}, \dots, A_{N-k+1}$ only depend on the seven parameters of the cosimulation test model, ρ is also a function of these seven parameters, only.

It should finally be stressed that the implicit coupling scheme presented above does only require one corrector step, since—due to the linearity of the problem—the gradients are constant, see Eq. (13). For nonlinear problems, the predictor/corrector approach described above would be semi-implicit (see Ref. [28]) and a corrector iteration with several corrector steps would be necessary in order to obtain a full-implicit method.

2.1.2 Explicit Cosimulation Approach. For the explicit coupling approach only one explicit integration step is required, which is identical with the predictor step in Sec. 2.1.1. Steps 2 and 3 of Sec. 2.1.1 are omitted.

Step 1: Explicit Integration Step

- An analytical integration of subsystem 1 and subsystem 2 from T_N to \bar{T}_{N+1} with initial conditions (8a) and with the extrapolation polynomial

$$\bar{\lambda}_c^p(\bar{t}) = P_{\bar{\lambda}_c}^p[(\bar{T}_N, \bar{\lambda}_{c,N}), (\bar{T}_{N-1}, \bar{\lambda}_{c,N-1}), \dots, (\bar{T}_{N-k}, \bar{\lambda}_{c,N-k}); \bar{t}] \quad (21)$$

yields the following state variables at the macrotime point \bar{T}_{N+1} :

$$\begin{aligned} x_{1,N+1} &= x_{1,N+1}(\bar{\lambda}_{c,N}, \bar{\lambda}_{c,N-1}, \dots, \bar{\lambda}_{c,N-k}, z_N) \\ \bar{v}_{1,N+1} &= \bar{v}_{1,N+1}(\bar{\lambda}_{c,N}, \bar{\lambda}_{c,N-1}, \dots, \bar{\lambda}_{c,N-k}, z_N) \\ x_{2,N+1} &= x_{2,N+1}(\bar{\lambda}_{c,N}, \bar{\lambda}_{c,N-1}, \dots, \bar{\lambda}_{c,N-k}, z_N) \\ \bar{v}_{2,N+1} &= \bar{v}_{2,N+1}(\bar{\lambda}_{c,N}, \bar{\lambda}_{c,N-1}, \dots, \bar{\lambda}_{c,N-k}, z_N) \end{aligned} \quad (22)$$

Making use of the coupling conditions at the macrotime points $\bar{T}_N, \dots, \bar{T}_{N-k}$, see Eq. (18), the coupling forces $\bar{\lambda}_{c,N}, \dots, \bar{\lambda}_{c,N-k}$ in Eq. (22) can be substituted, which yields relationships of the form

$$\begin{aligned} x_{1,N+1} &= x_{1,N+1}(z_N, z_{N-1}, \dots, z_{N-k}) \\ \bar{v}_{1,N+1} &= \bar{v}_{1,N+1}(z_N, z_{N-1}, \dots, z_{N-k}) \\ x_{2,N+1} &= x_{2,N+1}(z_N, z_{N-1}, \dots, z_{N-k}) \\ \bar{v}_{2,N+1} &= \bar{v}_{2,N+1}(z_N, z_{N-1}, \dots, z_{N-k}) \end{aligned} \quad (23)$$

As in the case of the implicit approach, Eq. (23) represents a system of four coupled linear recurrence equations. According to Sec. 2.1.1, this system can symbolically be written as

$$z_{N+1} + A_N \cdot z_N + \cdots + A_{N-k} \cdot z_{N-k} = 0 \quad (24)$$

Like in the case of implicit solver coupling, the matrices $A_N, \dots, A_{N-k} \in \mathbb{R}^{4 \times 4}$ are real-valued and constant. Again, they only depend on the seven parameters of the cosimulation test model, see Eq. (5). It should, however, be stressed that—although the same notation is used—the matrices A_N, \dots, A_{N-k} in Eq. (24) are not identical with the corresponding matrices in Eq. (20).

2.2 Force/Displacement-Coupling

2.2.1 Implicit Cosimulation Approach. For the case that the cosimulation test model is decomposed by a force/displacement-coupling approach, subsystem 1 will be a force-driven and subsystem 2 a base-point excited single-mass oscillator as illustrated in Fig. 3. Applying a force/displacement-decomposition, the coupling force λ_c is replaced in subsystem 2 with the help of the coupling condition (7c). Due to the fact that the state variables x_1 and v_1 are unknown in subsystem 2, they are replaced by two additional coupling variables, which are denoted by \tilde{x}_1 and \tilde{v}_1 . The introduction of two additional coupling variables entails the definition of two additional coupling conditions, namely, $g_{cx_1} := \tilde{x}_1 - x_1 = 0$ and $g_{cv_1} := \tilde{v}_1 - v_1 = 0$.

The semi-explicit index-1 DAE system, which describes the decomposed system, reads in dimensionless form

Subsystem 1:

$$\begin{aligned} x'_1 &= \bar{v}_1 \\ \bar{v}'_1 &= -\bar{c}_1 \cdot x_1 - \bar{d}_1 \cdot \bar{v}_1 + \bar{\lambda}_c \end{aligned} \quad (25a)$$

Subsystem 2:

$$\begin{aligned} x'_2 &= \bar{v}_2 \\ \bar{v}'_2 &= -\frac{\alpha_{c21}}{\alpha_{m21}} \cdot \bar{c}_1 \cdot x_2 - \frac{\alpha_{d21}}{\alpha_{m21}} \cdot \bar{d}_1 \cdot \bar{v}_2 - \frac{\alpha_{cc1}}{\alpha_{m21}} \cdot \bar{c}_1 \cdot (x_2 - \tilde{x}_1) \\ &\quad - \frac{\alpha_{dc1}}{\alpha_{m21}} \cdot \bar{d}_1 \cdot (\bar{v}_2 - \tilde{v}_1) \end{aligned} \quad (25b)$$

Coupling conditions:

$$\begin{aligned} \bar{g}_{c\lambda} &:= \bar{\lambda}_c - \alpha_{cc1} \cdot \bar{c}_1 \cdot (x_2 - x_1) - \alpha_{dc1} \cdot \bar{d}_1 \cdot (\bar{v}_2 - \bar{v}_1) = 0 \\ \bar{g}_{cx_1} &:= \tilde{x}_1 - x_1 = 0 \\ \bar{g}_{cv_1} &:= \tilde{v}_1 - v_1 = 0 \end{aligned} \quad (25c)$$

Like in Sec. 2.1.1, we consider the general macrostep from \bar{T}_N to \bar{T}_{N+1} to derive the governing recurrence equations system for the force/displacement-coupling approach. Again, we assume that at the beginning of the macrotime step, the state and the coupling variables are known

$$\begin{aligned} x_1(\bar{t} = \bar{T}_N) &= x_{1,N}, \quad \bar{v}_1(\bar{t} = \bar{T}_N) = \bar{v}_{1,N} \\ x_2(\bar{t} = \bar{T}_N) &= x_{2,N}, \quad \bar{v}_2(\bar{t} = \bar{T}_N) = \bar{v}_{2,N} \end{aligned} \quad (26a)$$

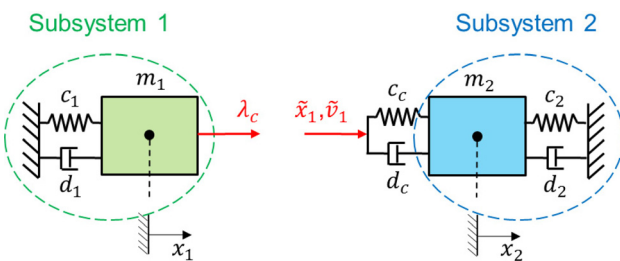


Fig. 3 Cosimulation test model: force/displacement-coupling approach

$$\begin{aligned} \bar{\lambda}_c(\bar{t} = \bar{T}_N) &= \bar{\lambda}_{c,N}, \quad \tilde{x}_1(\bar{t} = \bar{T}_N) = \tilde{x}_{1,N}, \quad \tilde{v}_1(\bar{t} = \bar{T}_N) = \tilde{v}_{1,N} \\ \end{aligned} \quad (26b)$$

For higher order approximation ($k > 0$), the coupling variables at the previous macrotime points are also assumed to be known.

Step 1: Predictor Step

- If we analytically integrate subsystem 1 and subsystem 2 from \bar{T}_N to \bar{T}_{N+1} with initial conditions (26a) and with the predictor (extrapolation) polynomials $\bar{\lambda}_c^p(\bar{t})$, $\bar{x}_1^p(\bar{t})$ and $\bar{v}_1^p(\bar{t})$, we get the following predicted state variables at the macrotime point \bar{T}_{N+1}

$$\begin{aligned} x_{1,N+1}^p &= x_{1,N+1}^p(\bar{\lambda}_{c,N}, \bar{\lambda}_{c,N-1}, \dots, \bar{\lambda}_{c,N-k}, z_N) \\ \bar{v}_{1,N+1}^p &= \bar{v}_{1,N+1}^p(\bar{\lambda}_{c,N}, \bar{\lambda}_{c,N-1}, \dots, \bar{\lambda}_{c,N-k}, z_N) \\ x_{2,N+1}^p &= x_{2,N+1}^p(\tilde{u}_{2,N}, \tilde{u}_{2,N-1}, \dots, \tilde{u}_{2,N-k}, z_N) \\ \bar{v}_{2,N+1}^p &= \bar{v}_{2,N+1}^p(\tilde{u}_{2,N}, \tilde{u}_{2,N-1}, \dots, \tilde{u}_{2,N-k}, z_N) \end{aligned} \quad (27)$$

where the vectors $\tilde{u}_{2,N} = (\tilde{x}_{1,N} \ \tilde{v}_{1,N})^T$, $\tilde{u}_{2,N-1} = (\tilde{x}_{1,N-1} \ \tilde{v}_{1,N-1})^T, \dots, \tilde{u}_{2,N-k} = (\tilde{x}_{1,N-k} \ \tilde{v}_{1,N-k})^T$ collect the coupling variables for subsystem 2 at the current and previous macrotime points.

Step 2: Calculation of Corrected Coupling Variables

- An analytical integration of subsystem 1 and subsystem 2 from \bar{T}_N to \bar{T}_{N+1} with initial conditions (26a) and with the interpolation polynomials $\bar{\lambda}_c^*(\bar{t})$, $\bar{x}_1^*(\bar{t})$, and $\bar{v}_1^*(\bar{t})$, yields the following state variables at the macrotime point \bar{T}_{N+1} :

$$\begin{aligned} x_{1,N+1}^* &= x_{1,N+1}^*(\bar{\lambda}_{c,N+1}^*, \bar{\lambda}_{c,N}, \dots, \bar{\lambda}_{c,N-k+1}, z_N) \\ \bar{v}_{1,N+1}^* &= \bar{v}_{1,N+1}^*(\bar{\lambda}_{c,N+1}^*, \bar{\lambda}_{c,N}, \dots, \bar{\lambda}_{c,N-k+1}, z_N) \\ x_{2,N+1}^* &= x_{2,N+1}^*(\tilde{u}_{2,N+1}^*, \tilde{u}_{2,N}, \dots, \tilde{u}_{2,N-k+1}, z_N) \\ \bar{v}_{2,N+1}^* &= \bar{v}_{2,N+1}^*(\tilde{u}_{2,N+1}^*, \tilde{u}_{2,N}, \dots, \tilde{u}_{2,N-k+1}, z_N) \end{aligned} \quad (28)$$

where $\bar{\lambda}_{c,N+1}^*$, $\tilde{x}_{1,N+1}^*$ and $\tilde{v}_{1,N+1}^*$ denote arbitrary coupling variables at the macrotime point \bar{T}_{N+1} .

- Inserting the state variables of Eq. (28) into the coupling conditions (25c) results in a linear equations system for the coupling variables, since the state vectors of Eq. (28) only linearly depend on the coupling variables and since the coupling conditions are linear. Solving this equations system for the coupling variables yields the corrected variables $\bar{\lambda}_{c,N+1}$, $\tilde{x}_{1,N+1}$ and $\tilde{v}_{1,N+1}$.

Step 3: Corrector Step

- Using interpolation polynomials with the corrected coupling variables $\bar{\lambda}_{c,N+1}$, $\tilde{x}_{1,N+1}$, and $\tilde{v}_{1,N+1}$, an analytical integration of both subsystems from \bar{T}_N to \bar{T}_{N+1} with initial conditions (26a) gives the corrected states

$$\begin{aligned} x_{1,N+1} &= x_{1,N+1}(\bar{\lambda}_{c,N+1}, \bar{\lambda}_{c,N}, \dots, \bar{\lambda}_{c,N-k+1}, z_N) \\ \bar{v}_{1,N+1} &= \bar{v}_{1,N+1}(\bar{\lambda}_{c,N+1}, \bar{\lambda}_{c,N}, \dots, \bar{\lambda}_{c,N-k+1}, z_N) \\ x_{2,N+1} &= x_{2,N+1}(\tilde{u}_{2,N+1}, \tilde{u}_{2,N}, \dots, \tilde{u}_{2,N-k+1}, z_N) \\ \bar{v}_{2,N+1} &= \bar{v}_{2,N+1}(\tilde{u}_{2,N+1}, \tilde{u}_{2,N}, \dots, \tilde{u}_{2,N-k+1}, z_N) \end{aligned} \quad (29)$$

By evaluating the coupling conditions (25c) at the $k+1$ macrotime points \bar{T}_{N+1} , $\bar{T}_N, \dots, \bar{T}_{N-k+1}$, the coupling variables in Eq. (29) can be eliminated, which yields a linear recurrence equations system of the forms (19) and (20), respectively.

2.2.2 Explicit Cosimulation Approach. Performing an explicit coupling approach, only one explicit integration step has to be

carried out. This explicit step is equivalent with the predictor step in Sec. 2.2.1. Replacing the coupling variables in Eq. (27) by means of the coupling conditions (25c), we obtain a linear recurrence equations system of the forms (23) and (24), respectively.

2.3 Displacement/Displacement-Coupling

2.3.1 Implicit Cosimulation Approach. When a displacement-displacement-coupling approach is used to decompose the two-mass oscillator, each subsystem is described by a base-point excited single-mass oscillator, see Fig. 4. For that purpose the coupling spring/damper system has to be duplicated, i.e., the coupling variable $\tilde{\lambda}_c$ is replaced in both subsystems with the help of the coupling condition (7c). Compared with the force/force-coupling approach, four coupling variables and in consequence four coupling conditions have to be defined.

The semi-explicit index-1 DAE system characterizing the decomposed system reads as

Subsystem 1:

$$\begin{aligned} x'_1 &= \bar{v}_1 \\ \bar{v}'_1 &= -\bar{c}_1 \cdot x_1 - \bar{d}_1 \cdot \bar{v}_1 + \alpha_{cc1} \cdot \bar{c}_1 \cdot (\tilde{x}_2 - x_1) \\ &\quad + \alpha_{dc1} \cdot \bar{d}_1 \cdot (\tilde{v}_2 - \bar{v}_1) \end{aligned} \quad (30a)$$

Subsystem 2:

$$\begin{aligned} x'_2 &= \bar{v}_2 \\ \bar{v}'_2 &= -\frac{\alpha_{c21}}{\alpha_{m21}} \cdot \bar{c}_1 \cdot x_2 - \frac{\alpha_{d21}}{\alpha_{m21}} \cdot \bar{d}_1 \cdot \bar{v}_2 - \frac{\alpha_{cc1}}{\alpha_{m21}} \cdot \bar{c}_1 \cdot (x_2 - \tilde{x}_1) \\ &\quad - \frac{\alpha_{dc1}}{\alpha_{m21}} \cdot \bar{d}_1 \cdot (\bar{v}_2 - \tilde{v}_1) \end{aligned} \quad (30b)$$

Coupling conditions:

$$\begin{aligned} \bar{g}_{cx_1} &:= \tilde{x}_1 - x_1 = 0 \\ \bar{g}_{cv_1} &:= \tilde{v}_1 - \bar{v}_1 = 0 \\ \bar{g}_{cx_2} &:= \tilde{x}_2 - x_2 = 0 \\ \bar{g}_{cv_2} &:= \tilde{v}_2 - \bar{v}_2 = 0 \end{aligned} \quad (30c)$$

Once again, the general macrotime step from \bar{T}_N to \bar{T}_{N+1} is considered to obtain the recurrence equations system. The state and the coupling variables at the beginning of the macrostep are given by

$$x_1(\bar{t} = \bar{T}_N) = x_{1,N}, \quad \bar{v}_1(\bar{t} = \bar{T}_N) = \bar{v}_{1,N} \quad (31a)$$

$$x_2(\bar{t} = \bar{T}_N) = x_{2,N}, \quad \bar{v}_2(\bar{t} = \bar{T}_N) = \bar{v}_{2,N} \quad (31b)$$

$$\tilde{x}_1(\bar{t} = \bar{T}_N) = \tilde{x}_{1,N}, \quad \tilde{v}_1(\bar{t} = \bar{T}_N) = \tilde{v}_{1,N}$$

$$\tilde{x}_2(\bar{t} = \bar{T}_N) = \tilde{x}_{2,N}, \quad \tilde{v}_2(\bar{t} = \bar{T}_N) = \tilde{v}_{2,N}$$

Step 1: Predictor Step

- Using the initial conditions (31a) and the predictor (extrapolation) polynomials $\tilde{x}_1^p(\bar{t})$, $\tilde{v}_1^p(\bar{t})$, $\tilde{x}_2^p(\bar{t})$, and $\tilde{v}_2^p(\bar{t})$, an analytical integration of the two subsystems from \bar{T}_N to \bar{T}_{N+1} yields the predicted state variables at the macrotime point \bar{T}_{N+1}

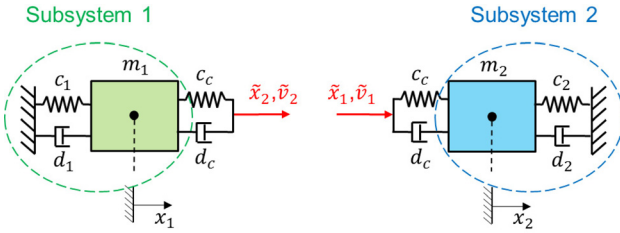


Fig. 4 Cosimulation test model: displacement/displacement-coupling approach

$$\begin{aligned} x_{1,N+1}^p &= x_{1,N+1}^p(\tilde{u}_{1,N}, \tilde{u}_{1,N-1}, \dots, \tilde{u}_{1,N-k}, z_N) \\ \bar{v}_{1,N+1}^p &= \bar{v}_{1,N+1}^p(\tilde{u}_{1,N}, \tilde{u}_{1,N-1}, \dots, \tilde{u}_{1,N-k}, z_N) \\ x_{2,N+1}^p &= x_{2,N+1}^p(\tilde{u}_{2,N}, \tilde{u}_{2,N-1}, \dots, \tilde{u}_{2,N-k}, z_N) \\ \bar{v}_{2,N+1}^p &= \bar{v}_{2,N+1}^p(\tilde{u}_{2,N}, \tilde{u}_{2,N-1}, \dots, \tilde{u}_{2,N-k}, z_N) \end{aligned} \quad (32)$$

where the vectors $\tilde{u}_{1,N} = (\tilde{x}_{2,N} \tilde{v}_{2,N})^T$, $\tilde{u}_{1,N-1} = (\tilde{x}_{2,N-1} \tilde{v}_{2,N-1})^T$, ..., $\tilde{u}_{1,N-k} = (\tilde{x}_{2,N-k} \tilde{v}_{2,N-k})^T$, and $\tilde{u}_{2,N} = (\tilde{x}_{1,N} \tilde{v}_{1,N})^T$, $\tilde{u}_{2,N-1} = (\tilde{x}_{1,N-1} \tilde{v}_{1,N-1})^T$, ..., $\tilde{u}_{2,N-k} = (\tilde{x}_{1,N-k} \tilde{v}_{1,N-k})^T$ collect the coupling variables at the current and previous macrotime points.

Step 2: Calculation of Corrected Coupling Variables

- By making use of the interpolation polynomials $\tilde{x}_1^*(\bar{t})$, $\tilde{v}_1^*(\bar{t})$, $\tilde{x}_2^*(\bar{t})$, and $\tilde{v}_2^*(\bar{t})$, an integration from \bar{T}_N to \bar{T}_{N+1} with initial conditions (31a) gives the following state variables at the macrotime point \bar{T}_{N+1}

$$\begin{aligned} x_{1,N+1}^* &= x_{1,N+1}^*(\tilde{u}_{1,N+1}^*, \tilde{u}_{1,N}, \dots, \tilde{u}_{1,N-k+1}, z_N) \\ \bar{v}_{1,N+1}^* &= \bar{v}_{1,N+1}^*(\tilde{u}_{1,N+1}^*, \tilde{u}_{1,N}, \dots, \tilde{u}_{1,N-k+1}, z_N) \\ x_{2,N+1}^* &= x_{2,N+1}^*(\tilde{u}_{2,N+1}^*, \tilde{u}_{2,N}, \dots, \tilde{u}_{2,N-k+1}, z_N) \\ \bar{v}_{2,N+1}^* &= \bar{v}_{2,N+1}^*(\tilde{u}_{2,N+1}^*, \tilde{u}_{2,N}, \dots, \tilde{u}_{2,N-k+1}, z_N) \end{aligned} \quad (33)$$

where $\tilde{x}_{1,N+1}^*$, $\tilde{v}_{1,N+1}^*$, $\tilde{x}_{2,N+1}^*$, and $\tilde{v}_{2,N+1}^*$ denote arbitrary coupling variables at the macrotime point \bar{T}_{N+1} .

- Inserting the state variables of Eq. (33) into the coupling conditions (30c) results in a linear equations system for the coupling variables, the solution of which yields the corrected coupling variables $\tilde{x}_{1,N+1}$, $\tilde{v}_{1,N+1}$, $\tilde{x}_{2,N+1}$, and $\tilde{v}_{2,N+1}$.

Step 3: Corrector Step

- Using interpolation polynomials with the corrected coupling variables $\tilde{x}_{1,N+1}$, $\tilde{v}_{1,N+1}$, $\tilde{x}_{2,N+1}$ and $\tilde{v}_{2,N+1}$, a subsystem integration from \bar{T}_N to \bar{T}_{N+1} with initial conditions (31a) yields the corrected states

$$\begin{aligned} x_{1,N+1} &= x_{1,N+1}(\tilde{u}_{1,N+1}, \tilde{u}_{1,N}, \dots, \tilde{u}_{1,N-k+1}, z_N) \\ \bar{v}_{1,N+1} &= \bar{v}_{1,N+1}(\tilde{u}_{1,N+1}, \tilde{u}_{1,N}, \dots, \tilde{u}_{1,N-k+1}, z_N) \\ x_{2,N+1} &= x_{2,N+1}(\tilde{u}_{2,N+1}, \tilde{u}_{2,N}, \dots, \tilde{u}_{2,N-k+1}, z_N) \\ \bar{v}_{2,N+1} &= \bar{v}_{2,N+1}(\tilde{u}_{2,N+1}, \tilde{u}_{2,N}, \dots, \tilde{u}_{2,N-k+1}, z_N) \end{aligned} \quad (34)$$

By evaluating the coupling conditions (30c) at the $k+1$ macrotime points \bar{T}_{N+1} , \bar{T}_N , ..., \bar{T}_{N-k+1} , the coupling variables in Eq. (34) can be eliminated, which gives again a linear recurrence equations system of the forms (19) and (20), respectively.

2.3.2 Explicit Cosimulation Approach. Performing the predictor step in Sec. 2.3.1, only, an explicit cosimulation scheme is obtained. Using the coupling conditions (30c) in order to replace the coupling variables in Eq. (32), one gets a linear recurrence equations system of the forms (23) and (24), respectively.

3 Results: Stability and Convergence Plots for Explicit and Implicit Cosimulation Methods

3.1 Stability Plots. As shown in Secs. 1 and 2, the spectral radius of the recurrence equations system, which characterizes the numerical stability of the underlying cosimulation method, depends on seven independent parameters. Fixing five parameters, the spectral radius can be plotted as a function of the remaining two parameters. The question will arise, if the seven parameters defined in Eq. (5) are most suitable for characterizing and representing the stability behavior of cosimulation methods. In accordance with the 2D stability plots for time integration schemes,

where the spectral radius of the recurrence equation is plotted as a function of $h\lambda_r$ and $h\lambda_i$, see Sec. 1, we choose a slightly modified set of parameters for representing 2D cosimulation stability plots.

In the following, we use the seven parameters

$$\begin{aligned} \bar{\lambda}_{r1} &= -\frac{\bar{d}_1}{2}, \quad \bar{\lambda}_{i1} = \frac{1}{2}\sqrt{4 \cdot \bar{c}_1 - \bar{d}_1^2}, \\ \alpha_{m21} &= \frac{m_2}{m_1}, \quad \alpha_{\lambda r21} = \frac{\bar{\lambda}_{r2}}{\bar{\lambda}_{r1}} = \frac{\alpha_{d21}}{\alpha_{m21}}, \\ \alpha_{\lambda i21} &= \frac{\bar{\lambda}_{i2}}{\bar{\lambda}_{i1}} = \frac{1}{\alpha_{m21}} \frac{\sqrt{4 \cdot \alpha_{m21} \cdot \alpha_{c21} \cdot \bar{c}_1 - \alpha_{d21}^2 \cdot \bar{d}_1^2}}{\sqrt{4 \cdot \bar{c}_1 - \bar{d}_1^2}}, \\ \alpha_{\lambda rc1} &= \frac{\alpha_{dc1}}{\alpha_m^*}, \quad \alpha_{\lambda ic1} = \frac{1}{\alpha_m^*} \frac{\sqrt{4 \cdot \alpha_m^* \cdot \alpha_{cc1} \cdot \bar{c}_1 - \alpha_{dc1}^2 \cdot \bar{d}_1^2}}{\sqrt{4 \cdot \bar{c}_1 - \bar{d}_1^2}} \quad \text{with} \\ \alpha_m^* &= 2 \frac{\alpha_{m21}}{1 + \alpha_{m21}} \end{aligned} \quad (35)$$

The physical interpretation of these parameters is straightforward. $\bar{\lambda}_{r1}$ and $\bar{\lambda}_{i1}$ represent the (modified/dimensionless) real and imaginary part of the eigenvalue of subsystem 1. The three parameters α_{m21} , $\alpha_{\lambda r21}$, and $\alpha_{\lambda i21}$ characterize subsystem 2. They describe the ratio of the subsystem masses as well as the ratio of the real and the imaginary part of the eigenvalue of subsystem 2 with respect to $\bar{\lambda}_{r1}$ and $\bar{\lambda}_{i1}$ (i.e., the ratio of the subsystem damping and the ratio of the subsystem frequencies). To characterize the coupling of the subsystems, the two parameters $\alpha_{\lambda rc1}$ and $\alpha_{\lambda ic1}$ are introduced. They may be interpreted as follows. For $c_1 = c_2 = d_1 = d_2 = 0$, the oscillation of the two masses is characterized by the eigenvalue $-(\alpha_{dc1} \cdot \bar{d}_1 / \alpha_m^*) + i \cdot (\sqrt{2 \cdot \alpha_m^* \cdot \alpha_{cc1} \cdot \bar{c}_1 - \alpha_{dc1}^2 \cdot \bar{d}_1^2} / \alpha_m^*)$.

The two parameters $\alpha_{\lambda rc1}$ and $\alpha_{\lambda ic1}$ are closely related with the ratio of the real and imaginary part of this eigenvalue with respect

to $\bar{\lambda}_{r1}$ and $\bar{\lambda}_{i1}$. However, a factor of 2 has artificially been introduced so that for the symmetric case ($m_1 = m_2$, $c_1 = c_2 = c_c$, and $d_1 = d_2 = d_c$) the parameters α_{m21} , $\alpha_{\lambda r21}$, $\alpha_{\lambda i21}$, $\alpha_{\lambda rc1}$ and $\alpha_{\lambda ic1}$ become 1.

In the following, stability plots are presented for the symmetric test model ($\alpha_{m21} = \alpha_{\lambda r21} = \alpha_{\lambda i21} = \alpha_{\lambda rc1} = \alpha_{\lambda ic1} = 1$). The parameters $\bar{\lambda}_{r1}$ and $\bar{\lambda}_{i1}$ are varied in the range $[-2, 0]$ and $[0, 10]$ for the implicit cosimulation schemes and in the range $[-2, 0]$ and $[0, 2]$ for the explicit methods. Specifying the seven parameters of the cosimulation test model, the spectral radius ρ of the corresponding recurrence equations system can be calculated. Note that the spectral radius can only be calculated numerically. The green circles in the plots indicate stable points, i.e., points for which $\rho \leq (1 + 10^{-10})$ holds. In order to reduce floating point errors, calculation of ρ has been carried out with 128 digits.

3.1.1 Implicit Cosimulation Approach. Stability plots for the implicit coupling schemes are collected in Figs. 5–7 for the force/force-, the force/displacement-, and the displacement/displacement-coupling approach. Plots have been generated for constant ($k = 0$), linear ($k = 1$), quadratic ($k = 2$), and cubic ($k = 3$) approximation polynomials. Except for the case $k = 0$, we observe that the region of instability will be increased if the polynomial degree is increased. Since the spectral radius can only be calculated numerically, it cannot be proven that the implicit schemes are A(α)-stable. However, further simulations, which are not shown here, indicate that the implicit schemes are also stable for very large values of $\bar{\lambda}_{r1}$ and $\bar{\lambda}_{i1}$. Figures 6 and 7 also exhibit that for the force/displacement- and especially for the displacement/displacement-coupling approach the region of instability for $k = 0$ is larger than for $k = 1$, which will not be the case if force/force-decomposition is applied.

3.1.2 Explicit Cosimulation Approach. Figures 8–10 collect 2D stability diagrams for the explicit cosimulation schemes. As in Sec. 3.1.1, plots for different approximation polynomials

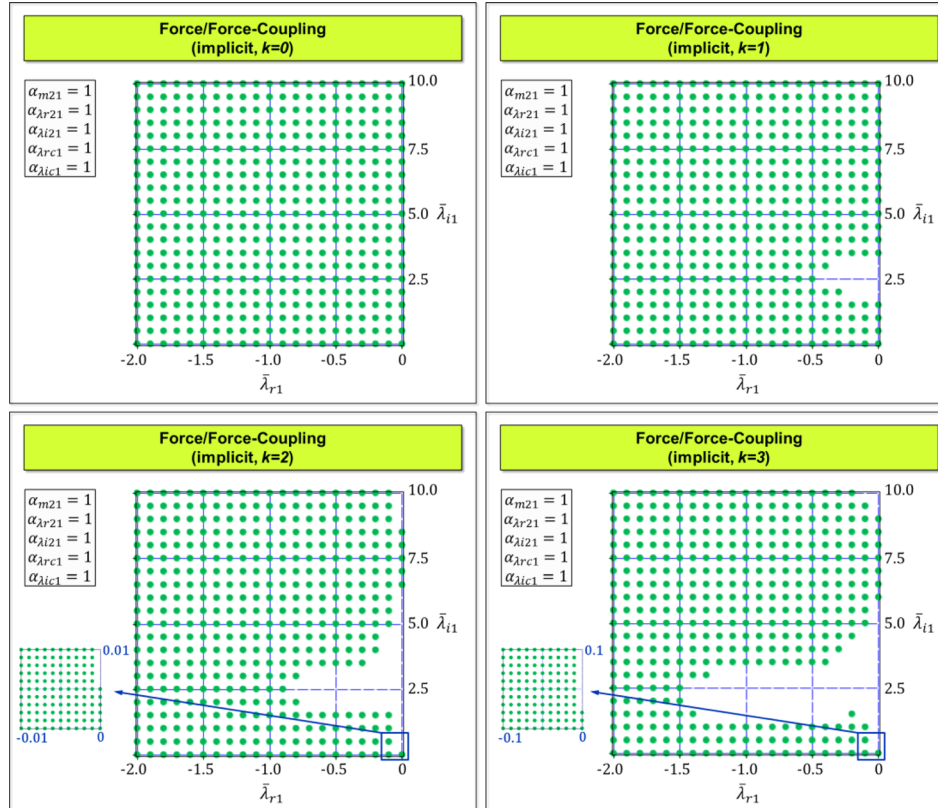


Fig. 5 Stability plots for the implicit cosimulation approach using force/force-decomposition

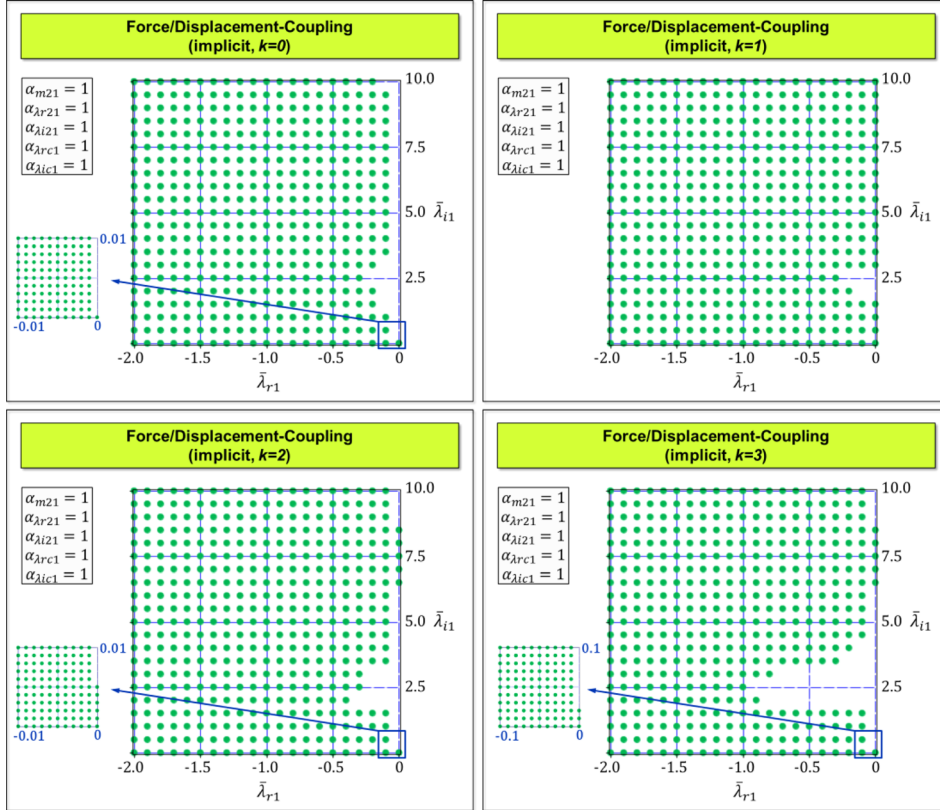


Fig. 6 Stability plots for the implicit cosimulation approach using force/displacement-decomposition

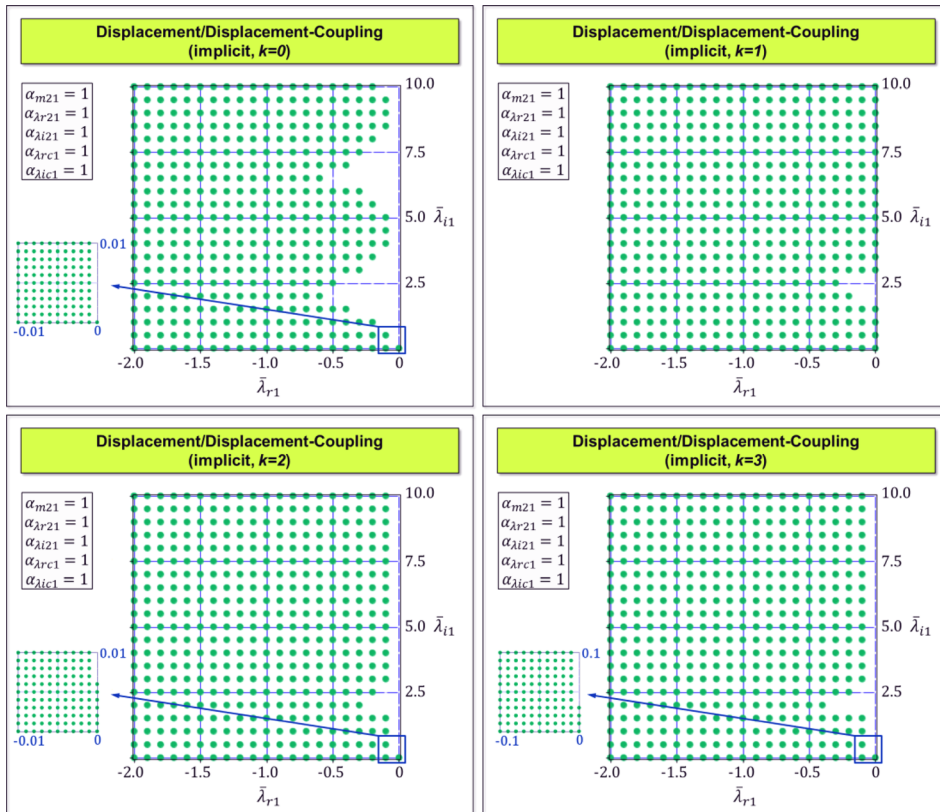


Fig. 7 Stability plots for the implicit cosimulation approach using displacement/displacement-decomposition

($k = 0, \dots, 3$) are presented for the three decomposition techniques. The reduced stability of the explicit schemes compared with their implicit counterparts is obvious. The higher the order of approximation is the more the stable region is reduced. For the considered set of parameters, the displacement/displacement-coupling approach exhibits the best stability behavior.

The above collected stability plots were generated with the symmetrical cosimulation test model. Further studies—which are not presented here—show that the five parameters α_{m21} , $\alpha_{\lambda r21}$, $\alpha_{\lambda i21}$, $\alpha_{\lambda rc1}$, and $\alpha_{\lambda ic1}$, which characterize the asymmetry of the cosimulation test model, may have a significant influence on the stability behavior of the explicit and the implicit cosimulation approaches.

3.2 Convergence Plots. In this section, convergence plots are collected for the symmetrical cosimulation test model ($m_1 = m_2 = 1$, $c_1 = c_2 = c_c = 1000$, $d_1 = d_2 = c_c = 10$). These plots may especially be interesting and helpful for the implementation of cosimulation methods with variable macrostep sizes, since therefore an error estimator for the local error is required. In the following, four different numerical errors are distinguished.

In this work, the relative global error for the position variables x_1/x_2 is calculated according to

$$\varepsilon_{\text{pos,glo}} = \sqrt{\frac{\sum_N (x_1(T_N) - x_{1,N})^2}{\sum_N (x_1(T_N) - x_{1,\text{mean}})^2} + \frac{\sum_N (x_2(T_N) - x_{2,N})^2}{\sum_N (x_2(T_N) - x_{2,\text{mean}})^2}}$$

with $x_{1,\text{mean}} = \sum_N \frac{x_1(T_N)}{N_{\text{total}}}$ and $x_{2,\text{mean}} = \sum_N \frac{x_2(T_N)}{N_{\text{total}}}$

(36)

where the values $x_{1,N}/x_{2,N}$ term the cosimulation results (solution of the recurrence equations system) and $x_1(T_N)/x_2(T_N)$ the values of the analytical solution at the macrotime point T_N . N_{total} denotes the total number of macrosteps. Analogously, we calculate the global error $\varepsilon_{\text{vel,glo}}$ for the velocity variables v_1/v_2 and the corresponding local errors $\varepsilon_{\text{pos,loc}}$ and $\varepsilon_{\text{vel,loc}}$ for the position and velocity variables.

Figure 11 shows the errors $\varepsilon_{\text{pos,glo}}$, $\varepsilon_{\text{vel,glo}}$, $\varepsilon_{\text{pos,loc}}$, and $\varepsilon_{\text{vel,loc}}$ for the implicit force/force-coupling approach for $k = 0, 1, 2, 3$. It can be seen that the global errors $\varepsilon_{\text{pos,glo}}$ and $\varepsilon_{\text{vel,glo}}$ converge with $\mathcal{O}(H^{k+1})$; the magnitudes of the global error for the position and velocity variables are almost equal. The local errors $\varepsilon_{\text{pos,loc}}$ and $\varepsilon_{\text{vel,loc}}$ converge with $\mathcal{O}(H^{k+3})$ and $\mathcal{O}(H^{k+2})$, respectively; the error in the position variables is significantly smaller than the corresponding error in the velocity variables. Using the same test model parameters, the convergence plots for the force/displacement- and the displacement/displacement-coupling approach show a quite similar behavior (same convergence behavior and similar magnitudes).

Figure 12 depicts the global and local errors $\varepsilon_{\text{pos,glo}}$, $\varepsilon_{\text{vel,glo}}$, $\varepsilon_{\text{pos,loc}}$, and $\varepsilon_{\text{vel,loc}}$ for the explicit force/force-coupling approach for different approximation orders ($k = 0, 1, 2, 3$). The corresponding plots for the force/displacement- and the displacement/displacement-coupling approach are quite similar (same convergence behavior and similar magnitudes) for the considered test model parameters and are therefore not shown here. The basic convergence behavior of the explicit approaches is quite similar to the implicit methods. Comparing the explicit with the implicit schemes, we observe—especially for higher approximation orders—larger errors for the explicit cosimulation methods.

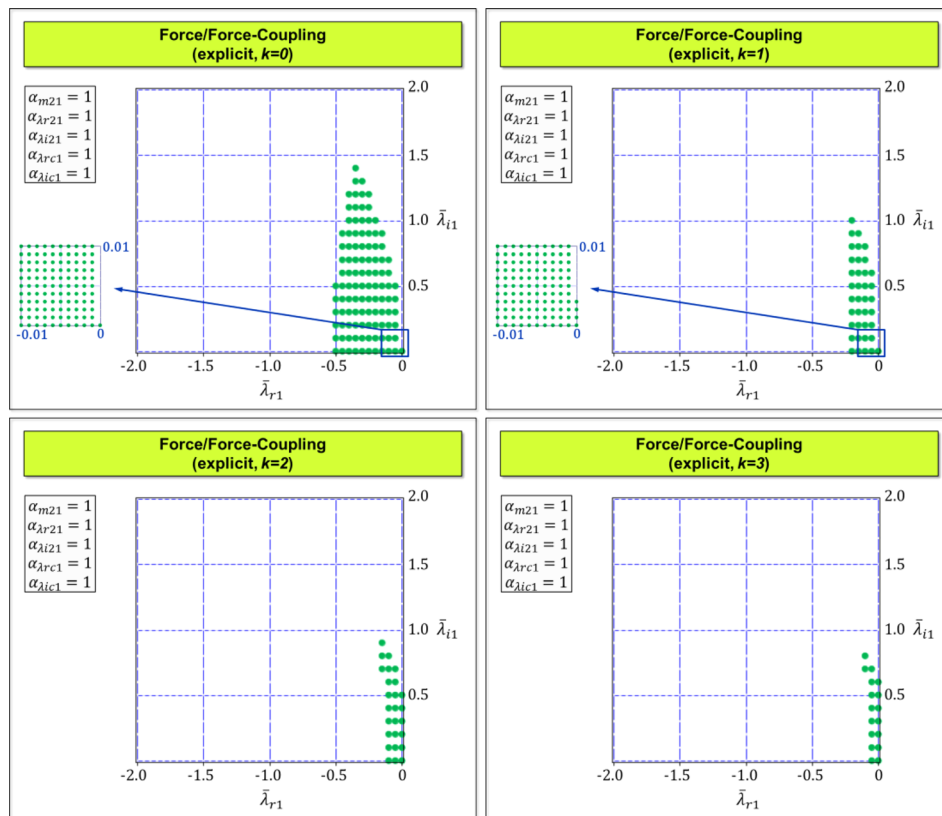


Fig. 8 Stability plots for the explicit cosimulation approach using force/force-decomposition

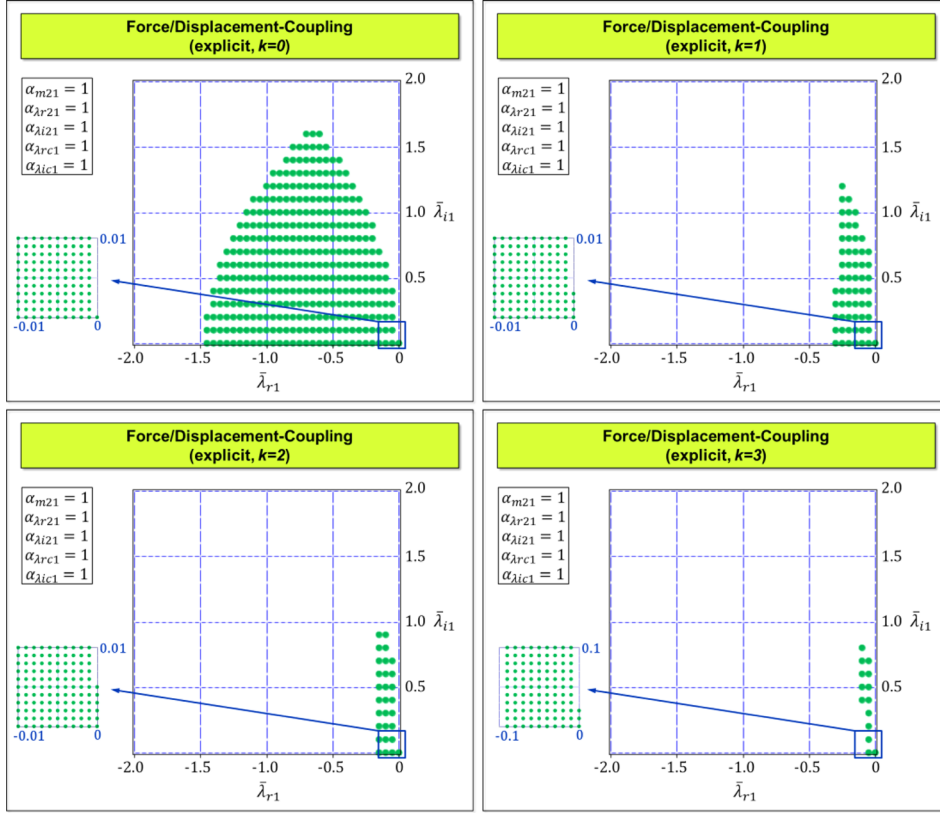


Fig. 9 Stability plots for the explicit cosimulation approach using force/displacement-decomposition

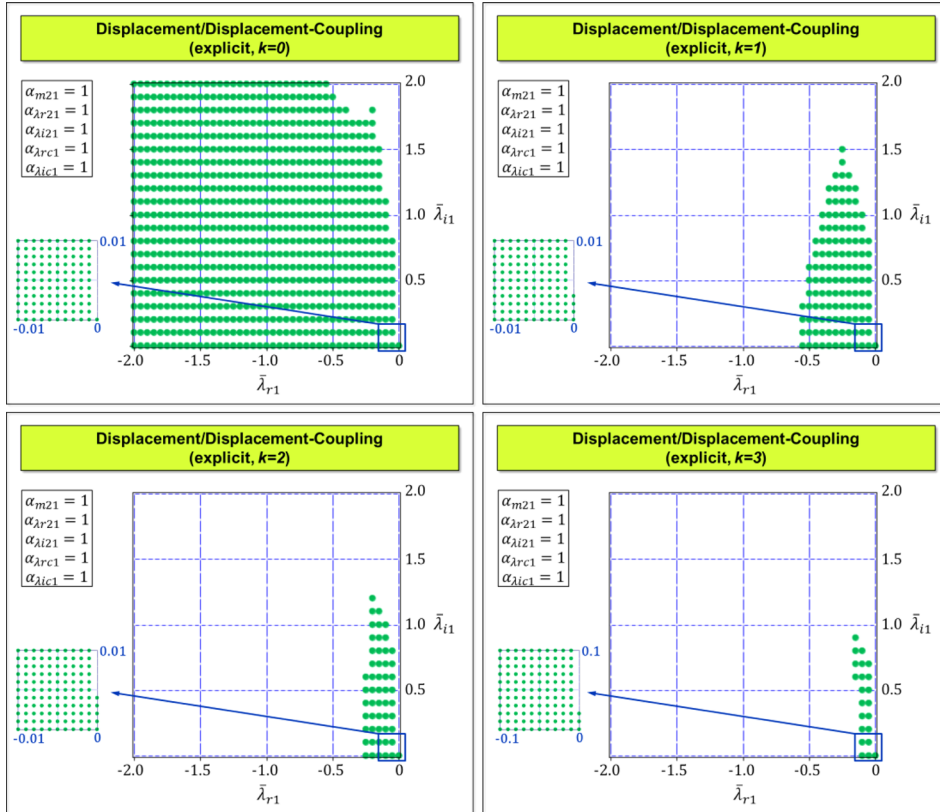


Fig. 10 Stability plots for the explicit cosimulation approach using displacement/displacement-decomposition

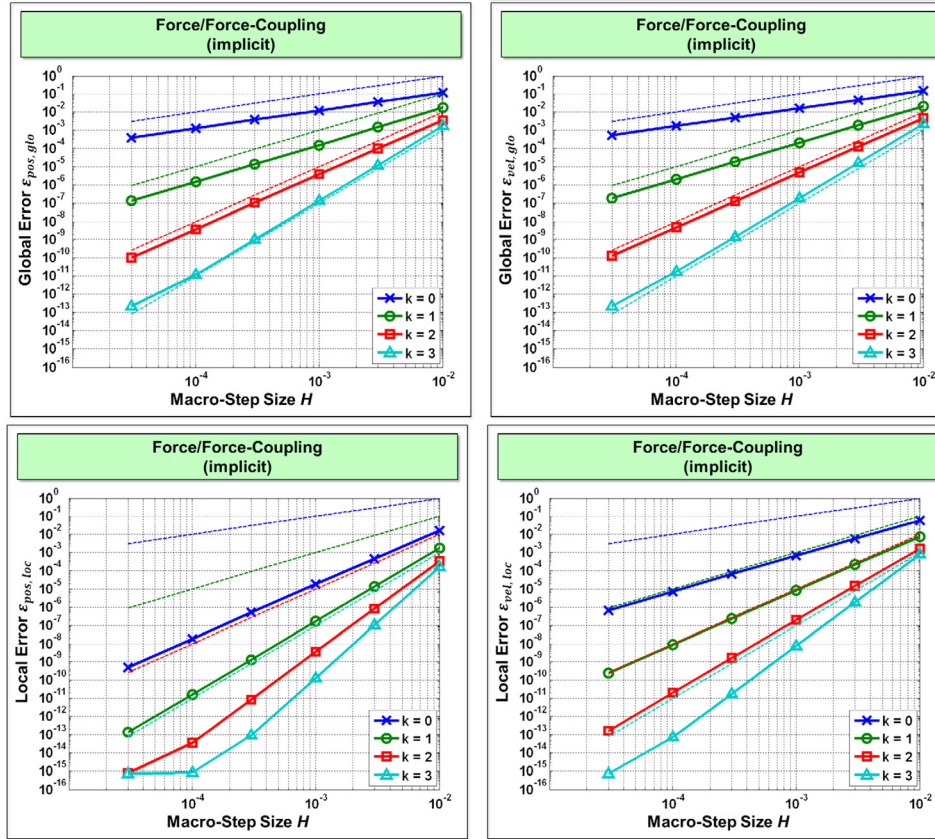


Fig. 11 Convergence plots for the implicit cosimulation approach using force/force-decomposition

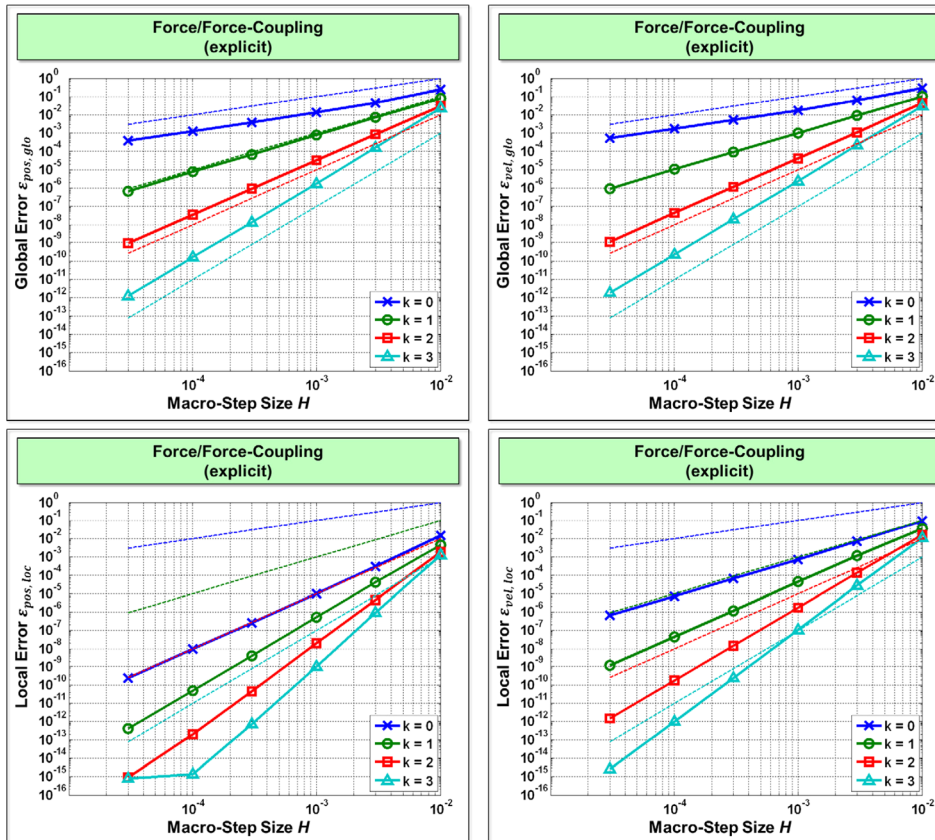


Fig. 12 Convergence plots for the explicit cosimulation approach using force/force-decomposition

4 Conclusions

The analysis of the numerical stability of cosimulation methods is inherently related with the definition of a test model. The most obvious cosimulation test model is the linear two-mass oscillator, whose stability behavior is characterized by seven independent parameters. Discretizing the test model with a cosimulation approach yields a linear homogenous system of recurrence equations. The spectral radius of this recurrence system characterizes the stability of the cosimulation method. In order to compare different cosimulation approaches, 2D stability plots are convenient. Therefore, five of the seven parameters are fixed so that the spectral radius can be depicted as a function of the remaining two parameters.

For illustrating the stability behavior of time integration schemes, usually real and imaginary part (multiplied by step size h) of the eigenvalue in Dahlquist's test equation are used as axis for the 2D stability plots. Accordingly, the modified real and imaginary part of the eigenvalue of subsystem 1 were used as axis for the 2D cosimulation stability plots in this paper. The remaining five parameters characterize the ratio of the subsystem masses, the ratio of real and imaginary part of subsystem 2 with respect to subsystem 1, and the ratio of real and imaginary part of the unfixed oscillator with respect to subsystem 1.

The results presented for the explicit cosimulation approaches show that the region of stability will successively be reduced if higher order approximation polynomials are used. Furthermore, it is shown that—at least for the chosen set of parameters—the displacement/displacement-decomposition approach exhibits a better stability behavior than cosimulation approaches based on force/displacement- and force/force-decomposition. As expected, implicit coupling schemes exhibit a significant better numerical stability than explicit schemes. Although A(α)-stability cannot be proven, calculations show that the implicit approaches are stable for very large values of $\bar{\lambda}_{r1}$ and $\bar{\lambda}_{i1}$.

Convergence studies show that the global errors in the position and velocity variables converge with $\mathcal{O}(H^{k+1})$. The local error in the position variables converges with $\mathcal{O}(H^{k+3})$, whereas the local error in the velocity variables converges with $\mathcal{O}(H^{k+2})$. The convergence behavior of the local errors may from the practical point of view be interesting for the implementation of an error estimator in connection with a macrostep size controller.

References

- [1] Datar, M., Stanculescu, I., and Negru, D., 2011, "A Co-Simulation Framework for Full Vehicle Analysis," Proceedings of the SAE 2011 World Congress, Detroit, MI, Apr. 12–14, SAE Technical Paper No. 2011-01-0516.
- [2] Datar, M., Stanculescu, I., and Negru, D., 2012, "A Co-Simulation Environment for High-Fidelity Virtual Prototyping of Vehicle Systems," *Int. J. Veh. Syst. Model. Test.*, **7**(1), pp. 54–72.
- [3] Liao, Y. G., and Du, H. I., 2001, "Co-Simulation of Multi-Body-Based Vehicle Dynamics and an Electric Power Steering Control System," *Proc. Inst. Mech. Eng. K*, **215**(3), pp. 141–151.
- [4] Negru, N., Melanz, D., Mazhar, H., Lamb, D., and Jayakumar, P., 2013, "Investigating Through Simulation the Mobility of Light Tracked Vehicles Operating on Discrete Granular Terrain," *SAE Int. J. Passeng. Cars Mech. Syst.*, **6**(1), pp. 369–381.
- [5] Carstens, V., Kemme, R., and Schmitt, S., 2003, "Coupled Simulation of Flow-Structure Interaction in Turbomachinery," *Aerospace Sci. Technol.*, **7**(4), pp. 298–306.
- [6] Dörfel, M. R., and Simeon, B., 2010, "Analysis and Acceleration of a Fluid-Structure Interaction Coupling Scheme," *Numerical Mathematics and Advanced Applications*, Springer, Berlin, Heidelberg, pp. 307–315.
- [7] Meynen, S., Mayer, J., and Schäfer, M., 2000, "Coupling Algorithms for the Numerical Simulation of Fluid-Structure-Interaction Problems," ECCOMAS 2000: European Congress on Computational Methods in Applied Sciences and Engineering, Barcelona, Spain, Sept. 11–14.
- [8] Schäfer, M., Yiğit, S., and Heck, M., 2006, "Implicit Partitioned Fluid-Structure Interaction Coupling," ASME Paper No. PVP2006-ICPVT11-93184.
- [9] Ambrosio, J., Pombo, J., Rauter, F., and Pereira, M., 2009, "A Memory Based Communication in the Co-Simulation of Multibody and Finite Element Codes for Pantograph-Catenary Interaction Simulation," *Multibody Dynamics: Computational Methods and Applications*, C. L. Bottasso, ed., Springer, pp. 231–252.
- [10] Ambrosio, J., Pombo, J., Pereira, M., Antunes, P., and Mosca, A., 2012, "A Computational Procedure for the Dynamic Analysis of the Catenary-Pantograph Interaction in High-Speed Trains," *J. Theor. Appl. Mech.*, **50**(3), pp. 681–699.
- [11] Busch, M., and Schweizer, B., 2012, "Coupled Simulation of Multibody and Finite Element Systems: An Efficient and Robust Semi-Implicit Coupling Approach," *Arch. Appl. Mech.*, **82**(6), pp. 723–741.
- [12] Nayra, M., Cuadrado, J., Dopico, D., and Lugris, U., 2011, "An Efficient Unified Method for the Combined Simulation of Multibody and Hydraulic Dynamics: Comparison With Simplified and Co-Integration Approaches," *Arch. Mech. Eng.*, **58**(2), pp. 223–243.
- [13] Schimoll, R., and Schweizer, B., 2011, "Co-Simulation of Multibody and Hydraulic Systems: Comparison of Different Coupling Approaches," *Multibody Dynamics 2011, ECCOMAS Thematic Conference*, J. C. Samin and P. Fisette, eds., Brussels, Belgium, July 4–7, pp. 1–13.
- [14] Eberhard, P., Gaugel, T., Heisel, U., and Storchak, M., 2008, "A Discrete Element Material Model Used in a Co-Simulated Charpy Impact Test and for Heat Transfer," *Proceedings 1st International Conference on Process Machine Interactions*, Hannover, Germany, Sept. 3–4.
- [15] Lehnart, A., Fleissner, F., and Eberhard, P., 2009, "Using SPH in a Co-Simulation Approach to Simulate Sloshing in Tank Vehicles," *Proceedings SPHERIC4*, Nantes, France, May 27–29.
- [16] Spreng, F., Eberhard, P., and Fleissner, F., 2013, "An Approach for the Coupled Simulation of Machining Processes Using Multibody System and Smoothed Particle Hydrodynamics Algorithms," *Theor. Appl. Mech. Lett.*, **3**(1): p. 8-013005.
- [17] Friedrich, M., and Ulbrich, H., 2010, "A Parallel Co-Simulation for Mechatronic Systems," *Proceedings of The 1st Joint International Conference on Multibody System Dynamics, IMSD 2010*, Lappeenranta, Finland, May 25–27.
- [18] Gonzalez, F., Gonzalez, M., and Cuadrado, J., 2009, "Weak Coupling of Multibody Dynamics and Block Diagram Simulation Tools," *ASME Paper No. DETC2009-86653*.
- [19] Helduser, S., Stuewing, M., Liebig, S., and Dronka, S., 2001, "Development of Electro-Hydraulic Actuators Using Linked Simulation and Hardware-in-the-Loop Technology," *Power Transmission and Motion Control*, C. Burrows and K. Edge, eds., Bath, UK, pp. 49–56.
- [20] Hippmann, G., Arnold, M., and Schittenhelm, M., 2005, "Efficient Simulation of Bush and Roller Chain Drives," *Proceedings of ECCOMAS Thematic Conference on Advances in Computational Multibody Dynamics*, J. Goicoeal, J. Cuadrado, and J. G. Orden, eds., Madrid, Spain, June 21–24, pp. 1–18.
- [21] Wuensche, S., Claub, C., Schwarz, P., and Winkler, F., 1997, "Electro-Thermal Circuit Simulation Using Simulator Coupling," *IEEE Trans. Very Large Scale Integr. Syst.*, **5**(3), pp. 277–282.
- [22] Gu, B., and Asada, H. H., 2004, "Co-Simulation of Algebraically Coupled Dynamic Subsystems Without Disclosure of Proprietary Subsystem Models," *ASME J. Dyn. Syst. Meas. Control*, **126**(1), pp. 1–13.
- [23] Kübler, R., and Schiehlen, W., 2000, "Two Methods of Simulator Coupling," *Math. Comput. Modell. Dyn. Syst.*, **6**(2), pp. 93–113.
- [24] Schweizer, B., and Lu, D., 2014, "Predictor/Corrector Co-Simulation Approaches for Solver Coupling With Algebraic Constraints," *ZAMM-J. Appl. Math. Mech.*, (in press).
- [25] Schweizer, B., and Lu, D., 2014, "Co-Simulation Methods for Solver Coupling With Algebraic Constraints: Semi-Implicit Coupling Techniques," *Proceedings of The 3rd Joint International Conference on Multibody System Dynamics and The 7th Asian Conference on Multibody Dynamics, IMSD 2014, ACMD 2014*, Bexco, Busan, Korea, June 30–July 3.
- [26] Schweizer, B., and Lu, D., 2014, "Stabilized Index-2 Co-Simulation Approach for Solver Coupling With Algebraic Constraints," *Multibody Syst. Dyn.*, (in press).
- [27] Busch, M., and Schweizer, B., 2010, "Numerical Stability and Accuracy of Different Co-Simulation Techniques: Analytical Investigations Based on a 2-DOF Test Model," *Proceedings of The 1st Joint International Conference on Multibody System Dynamics, IMSD 2010*, Lappeenranta, Finland, May 25–27.
- [28] Schweizer, B., and Lu, D., 2014, "Semi-Implicit Co-Simulation Approach for Solver Coupling," *Arch. Appl. Mech.*, (in press).
- [29] Busch, M., and Schweizer, B., 2011, "An Explicit Approach for Controlling the Macro-Step Size of Co-Simulation Methods," *Proceedings of The 7th European Nonlinear Dynamics, ENOC 2011*, Rome, Italy, July 24–29.
- [30] Verhoeven, A., Tasic, B., Beelen, T. G. J., ter Maten, E. J. W., and Mattheij, R. M. M., 2008, "BDF Compound-Fast Multirate Transient Analysis With Adaptive Stepsize Control," *J. Numer. Anal. Ind. Appl. Math.*, **3**(3–4), pp. 275–297.
- [31] Hairer, E., Norsett, S. P., and Wanner, G., 2009, *Solving Ordinary Differential Equations I: Nonstiff Problems*, 3rd ed., Springer, Berlin.
- [32] Hairer, E., and Wanner, G., 2010, *Solving Ordinary Differential Equations II: Stiff and Differential-Algebraic Problems*, 2nd ed., Springer, Berlin.
- [33] Gear, C. W., and Wells, D. R., 1984, "Multirate Linear Multistep Methods," *BIT Numer. Math.*, **24**(4), pp. 484–502.